Analytical Chemistry

Supporting Information

Photothermal Microfluidic Sensing Platform Using Near-Infrared Laser-Driven Multiplexed Dual-Mode Visual Quantitative Readout

Guanglei Fu,*[a] Yabin Zhu,[a] Kui Xu,[a] Weihua Wang,[b] Ruixia Hou,[a] and Xiujun Li*[c]

[a]Biomedical Engineering Research Center, Medical School of Ningbo University, Ningbo, Zhejiang 315211, P. R. China

[b]The Affiliated Hospital of Medical School of Ningbo University, Ningbo, Zhejiang 315020, P. R. China

[c]Department of Chemistry and Biochemistry, University of Texas at El Paso, 500 West University Avenue, El Paso, Texas 79968, United States

*Corresponding Author

E-mail: fuguanglei@nbu.edu.cn; xli4@utep.edu

Table of Contents

Experimental Section

Materials and Instruments. Acrylamide (AcAm) was the product of Aladdin Bio-Chem Technology Co., Ltd (Shanghai, China). N,N,N',N'-tetramethylethylenediamine (TEMED) was obtained from Aladdin Bio-Chem Technology Co., Ltd (Shanghai, China). Red food dye was obtained from AmeriColor Corp (CA, USA). Bisacrylamide and ammoniumpersulfate (APS) were acquired from Sigma-Aldrich (MO, USA). Dextran 70 was purchased from Aladdin Bio-Chem Technology Co., Ltd (Shanghai, China). Whatman chromatography papers (Grade No. 1) were the products of GE Healthcare Worldwide (Shanghai, China). Silver nitrate was the product of Shandong XiYa Chemical Industry Co., Ltd (Shandong, China). Ultrapure water (18.2 MΩ cm) was collected from a Milli-Q purification system (Bedford, MA). UV-vis absorption spectroscopic characterization was performed by using a Shimadzu UV-1800 spectrophotometer (Shimadzu, Kyoto, Japan). Photographs of μPADs were taken with a Canon EOS 600D camera (Canon Inc., Tokyo, Japan). Fourier transformed infrared (FT-IR) spectroscopic characterization of the hydrogels was carried out on a Nicolet 380 FT-IR spectrometer (Thermo Scientific, USA). Scanning electron microscopic (SEM) characterization of the hydrogels was performed by utilizing a FEI Quanta 250 scanning electron microscope (FEI Co., OR, USA). Thermal images were taken by using a FLIR C2 thermal camera (FLIR Systems Inc., CA, USA). Unless otherwise stated, all other chemicals were of analytical grade and were used as received.

Synthesis of Blank and Photothermally Responsive Hydrogels. The blank NIPAM-AcAm hydrogels were synthesized *via* the radical polymerization method according to the literature.[1] In brief, NIPAM (299 mg), AcAm (21 mg), bisarylamide (8 mg) and dextran 70 (40 mg) were dissolved in 2.0 ml of ultrapure water. After the addition of 100 μL of APS solution (65 mM), the aqueous mixture was thoroughly purged with N_2 for 5.0 min. Afterwards, 24 μL of TEMED was added into the above solution to initiate the polymerization reaction, followed by rapid filling of the aqueous mixture into plastic syringes (1.0 mL). The syringes were then stored at room temperature for 12 h to perform the polymerization reaction. To remove unreacted chemicals in the hydrogels, the as-obtained hydrogel rods were first incubated in water bath at 55 ^{o}C for 20 min to induce their complete collapse. The collapsed hydrogels were then stored in water at room temperature to achieve the swelling to their initial shape. The above washing procedure was repeated 3 times.

The photothermally responsive hydrogels (i.e. PB-NIPAM-AcAm) were prepared through an in-situ synthesis route. Briefly, the blank NIPAM-AcAm hydrogels were incubated in water bath at 55 ^{o}C for 20 min to induce their structural collapse, followed by successive storage of the hydrogels in aqueous solutions (25 mM citric acid) of $FeCl_3$ and potassium ferrocyanide for 3.0 hours at room temperature, respectively. Afterwards, the hydrogels were thoroughly washed with deionized water. The collapsed hydrogels were stored overnight in aqueous dye solutions at room temperature to load dye solutions in the hydrogel matrix. Unless otherwise stated, the

concentration of $FeCl_3$ and potassium ferrocyanide used for synthesis of the composite hydrogel was 1.0 mM.

Before the loading of the hydrogels on μPADs, the as-obtained hydrogel rods of 6.0 mm in diameter were uniformly sliced into circular pieces of 2.0 mm in thickness, followed by drying of the hydrogel pieces on filter papers.

Fabrication of Photothermal μPAD. Patterns of μPADs were designed with the CorelDraw X4 software. The disk-like μPAD consisted of a central circular irradiation zone and multiple straight channels accessable to the irradiation zone. The central irradiation zone (2.0 cm in diameter) was composed of six circular inlets of 6.0 mm in diameter. Six straight channels of 2.5 mm in width and 5.0 cm in length were individually connected to corresponding inlets. The irradiation zone and channels were designed for multiplexed thermal image- and distance-based visual quantitative readout, respectively. Microfluidic hydrophobic barriers were printed on chromatography papers by using a wax printer (Xerox Phaser 8560, Fuji Xerox CO., LTD., Japan). The wax-printed chromatograph papers were heated in an oven for 3.0 min at 150 ^{o}C, followed by sealing of the back of the device with adhesive tapes.

On-Chip Distance- and Thermal Image-Based Visual Quantitative Readout. Thermal images of the μPADs were taken before and after the laser irradiation, which were quantitatively analyzed with the FLIR Tools software for thermal image-based readout. After 10 minutes upon removal of the laser irradiation, photographs of the

μPADs were taken to measure the travelling distance of dye solutions released in the channels.

Determination of Silver Ions in Real Environmental Water Samples. Aqueous solutions of Ag^+ were prepared with Britton-Robinson (B-R) buffer solutions (pH=7.2). The hydrogel pieces were incubated in different concentrations of standard Ag^+ solutions for 1.5 hours at room temperature, followed by loading of dye solutions into the hydrogels. The photothermal sensing performance of the hydrogels was then quantitatively analyzed using the dual-mode readout method on the μPAD. To evaluate the selectivity of the photothermal μPAD, the same concentration (i.e. 30 μM) of other metal ions, including Mg^{2+}, Cu^{2+}, Fe^{3+}, Zn^{2+}, Ca^{2+}, Ba^{2+} and Fe^{2+}, were determined in parallel to Ag^+. Real water samples collected from a local lake were used to validate the practical analytical application of the μPAD. 1.5 mL of the water samples (5-fold diluted with B-R buffer solutions) were spiked with 10 μL of different concentrations of standard Ag^+ solutions to prepare water samples with final Ag^+ concentrations of 5.0, 10 and 20 μM, respectively. The concentrations of Ag^+ were determined on the μPAD to calculate the analytical recoveries using the dual-mode readout method.

Results and Discussion

FTIR Characterization of Hydrogels. The freeze-dried hydrogels were ground into powders and characterized by Fourier transform infrared spectroscopy (FTIR). As can

be seen in Figure S1, the composite hydrogel exhibited an obvious stretching band at 2088 cm^{-1} that corresponded well with the CN stretching band in the [Fe^{II}–CN–Fe^{III}] structures in Prussian blue (PB),[2, 3] whereas no apparent stretching band was observed from the blank hydrogel in this region. The result confirmed the successful synthesis of PB in the composite hydrogel.

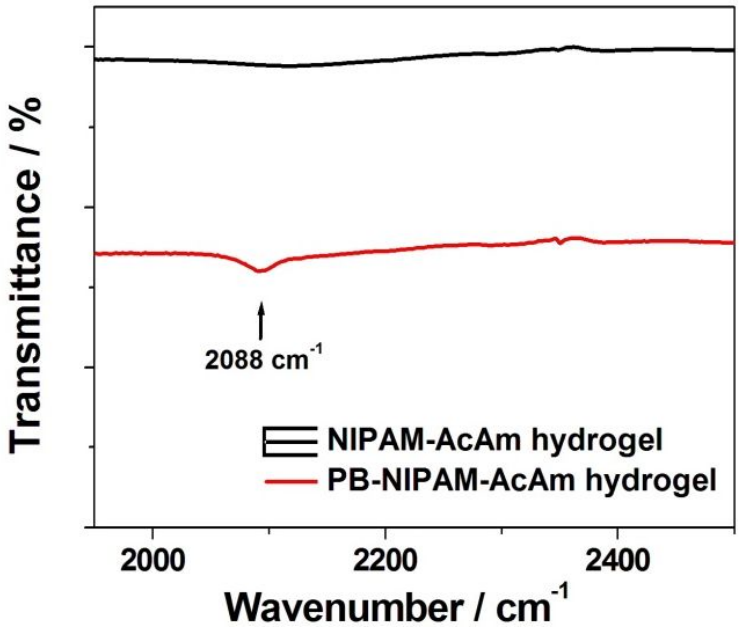

Figure S1. FTIR characterization of hydrogels. FTIR spectra of the blank (i.e., NIPAM-AcAm) and composite (i.e., PB-NIPAM-AcAm) hydrogels.

Optical Absorption Properties of PB and Red Dye in NIR Region. The optical absorption properties of PB nanoparticles (NPs) and red dye in the NIR region were studied by UV-vis absorption spectroscopy as shown in Figure S2. The aqueous dispersion of PB NPs showed strong optical absorption in the range of 500-1000 nm with the absorption peak at 710 nm, which can be ascribed to the charge transfer transition between Fe (II) and Fe (III) in PB NPs.[3, 4] In contrast, the red dye solution

showed no apparent optical absorption in the range of 600-1000 nm. Hence, under irradiation of an 808 nm laser, only PB served as the photothermally responsive element in the composite hydrogel without any photothermal interference from the red dye.

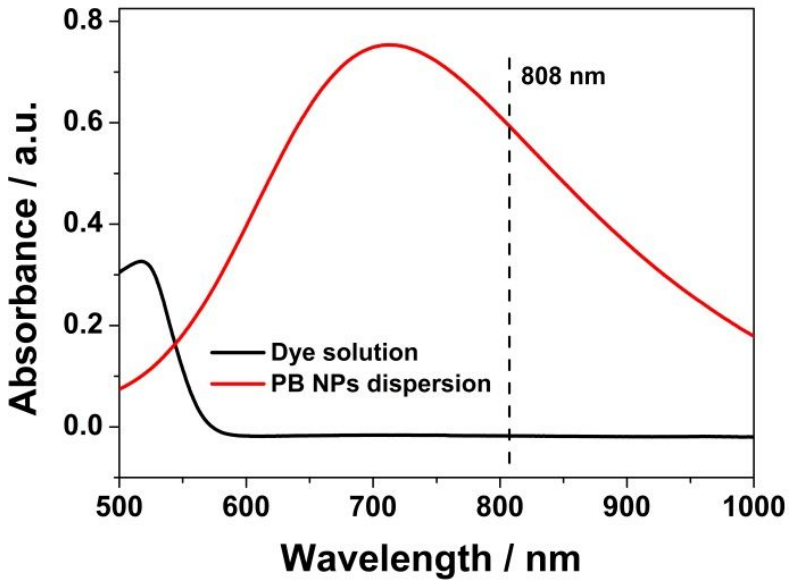

Figure S2. UV-vis absorption spectroscopic characterization of red dye and PB. UV-vis absorption spectra of red dye solution and aqueous dispersion of PB NPs (0.05 mg/mL).

Feasibility of Red Dye as On-Chip Quantitative Indicator of the Distance-Based Readout Method. On the μPAD, the capillary force can drive the flow of dye solutions in the channels, thus displaying visual red strips with quantitative lengths. Different volumes of the red dye solutions were pipetted to inlets of the disk-like μPAD to evaluate the feasibility of the read dye as the on-chip quantitative indicator of the distance-based readout method. As shown in Figure S3, the on-chip travelling distance of the dye solutions is proportional to the solution volume in the range from 2.0 to 20 μL at the capillary transport temperature of both 4.0 ^{o}C and 29 ^{o}C, indicating

the feasibility of the read dye as the on-chip quantitative indicator of the distance-based readout method on the μPAD. In addition, the effect of temperature on on-chip capillary transport of the dye solution was assessed using 4.0 °C as the control (*vs.* room temperature of around 29 °C). It was found that the control μPAD (Figure S3B) showed longer dye-travelling distance than that obtained at the room temperature (Figure S3A) at various volumes. Accordingly, the control calibration plot (Figure S3C) exhibited a higher slope than that obtained at the room temperature, illustrating a negative effect of temperature on on-chip transport distance of the dye solution because of the influence on surface tension of the dye solution.

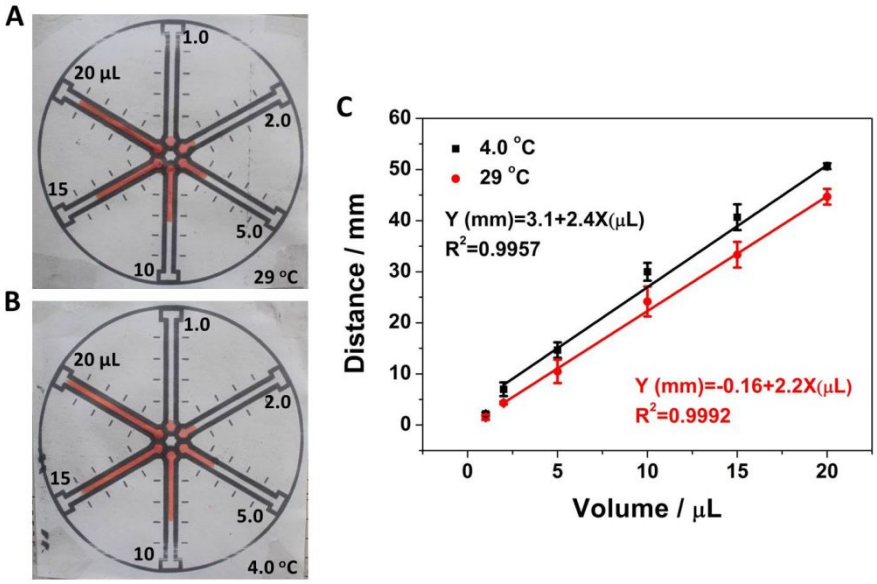

Figure S3. On-chip capillary force-driven travelling behavior of pure dye solution. (A) Photograph of the dye-loaded μPAD with the capillary transport at 29 °C; (B) Photograph of the control dye-loaded μPAD with the capillary transport at 4.0 °C; (C) Calibration plots of on-chip dye-travelling distance *vs.* volume of the dye solutions. Error bars represent standard deviations (n=3).

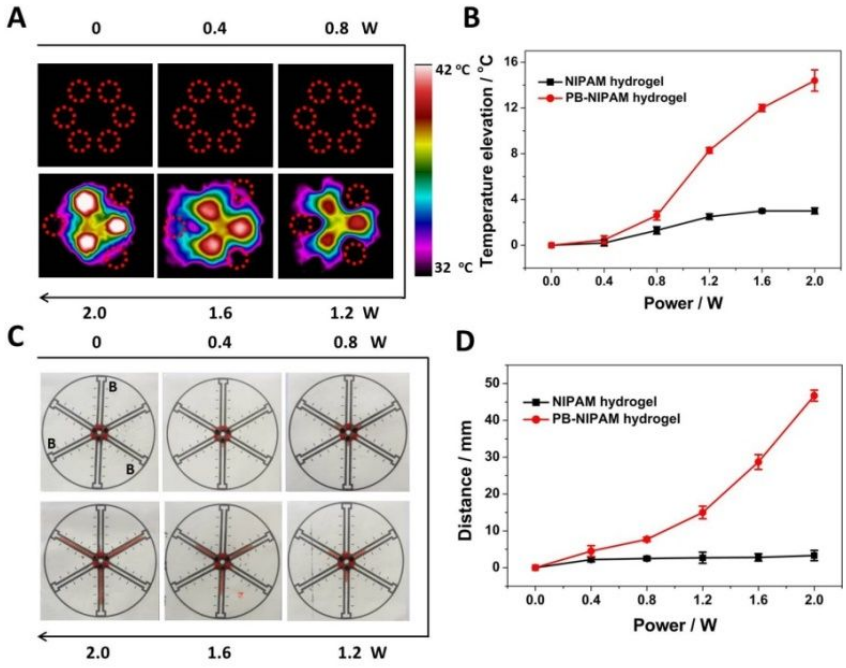

Figure S4. Effect of laser power on on-chip photothermal sensing performance of hydrogels. (A) Thermal images of the blank and composite hydrogels after the laser irradiation for 60 s at different laser powers; (B) Temperature elevations of the hydrogels after the irradiation; (C) Photographs of the hydrogel-loaded μPADs after the irradiation; (D) On-chip travelling distance of dye solutions as a function of laser power. Error bars represent standard deviations (n=3).

Effect of Laser Power on On-Chip Photothermal Sensing Performance of Hydrogels. The effect of laser power on photothermal sensing performance of the composite hydrogel was studied using the dual-mode readout method as shown in Figure S4. With the increase of laser power in the range from 0 to 2.0 W, the composite hydrogels showed progressively increased temperature due to the increasing photothermal effect of PB in the hydrogels. Irradiation of the composite hydrogel at a laser power of 2.0 W resulted in a dramatic temperature elevation of 14.4 °C, while the blank hydrogel exhibited a minor temperature elevation of 3.7 °C. In good agreement with the thermal image-based readout results, increasing

dye-travelling distance (i.e., 47 mm at 2.0 W) was observed from the composite hydrogels upon the increase of laser power, whereas the blank hydrogels exhibited minor dye-travelling distance of less than 3.3 mm at various laser powers. These results demonstrated a laser power-dependent character of the photothermal sensing performance of the composite hydrogel.

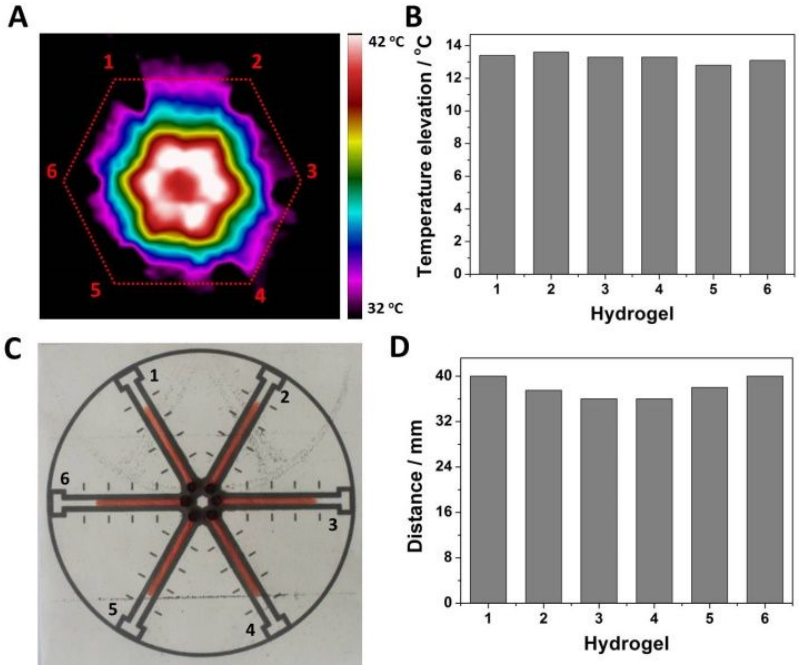

Figure S5. Reproducibility of on-chip photothermal sensing performance of composite hydrogel. (A) Thermal image of six pieces of the composite hydrogels synthesized from six independent batches after the laser irradiation for 50 s at a power density of 0.38 W·cm^{-2}; (B) Temperature elevations of the composite hydrogels after the irradiation; (C) Photograph of the hydrogel-loaded μPAD after the irradiation; (D) On-chip travelling distance of dye solutions after the irradiation.

Reproducibility of On-Chip Photothermal Sensing Performance of Hydrogels. To study the reproducibility of on-chip photothermal sensing performance of the composite hydrogel, the composite hydrogels prepared in parallel from independent

batches were irradiated for the same time on the μPAD. As can be seen in Figure S5, after the laser irradiation for 50 s at a power density of 0.38 W·cm^{-2}, uniform temperature elevations of six pieces of the composite hydrogels were monitored with a low relative standard deviation (RSD) of 2.0%. In addition, the composite hydrogels exhibited uniform on-chip dye-travelling distance with a relative standard deviation (RSD) of 4.8%. These results demonstrated good reproducibility of on-chip photothermal sensing performance of the composite hydrogel.

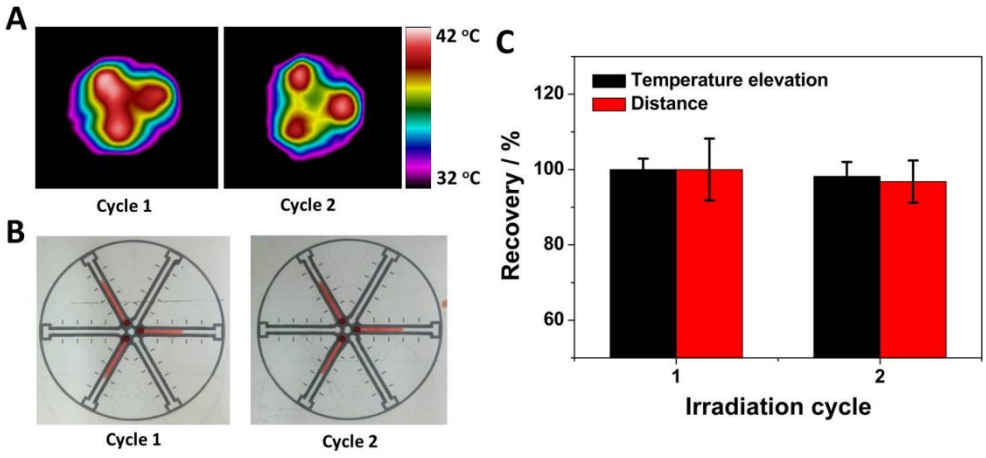

Figure S6. Recovery of on-chip photothermal sensing performance upon reusage of hydrogels. (A) Thermal images of the composite hydrogels after 2 cycles of laser irradiation for 40 s at a power density of 0.38 W·cm^{-2}; (B) Photographs of the hydrogel-loaded μPADs after the irradiation; (C) Temperature elevations of the hydrogels and on-chip travelling distance of dye solutions after the irradiation. Error bars represent standard deviations (n=3).

Recovery of On-Chip Photothermal Sensing Performance upon Reusage of Hydrogels. It had been reported that the structural phase transition of NIPAM-derived thermoresponsive hydrogels was completely reversible in response to external temperature changes. Herein, the recovery of on-chip photothermal sensing

performance of the composite hydrogel was investigated upon multiple cycles of reusage of the composite hydrogel, as shown in Figure S6. The composite hydrogels on the μPAD were treated by two cycles of reusage. In each cycle, the hydrogels were first irradiated for 40 s, followed by off-chip re-storage of the hydrogels in red dye solutions at room temperature to allow their thorough swelling. The composite hydrogels showed no distinct changes in both the thermal image- and distance-based readout results after the above treatment, suggesting remarkable recovery of on-chip photothermal sensing performance of the composite hydrogel on the μPAD. The good recovery can be attributed to the reversible phase-transition behavior of the composite hydrogel upon thermal stimulus.[5, 6]

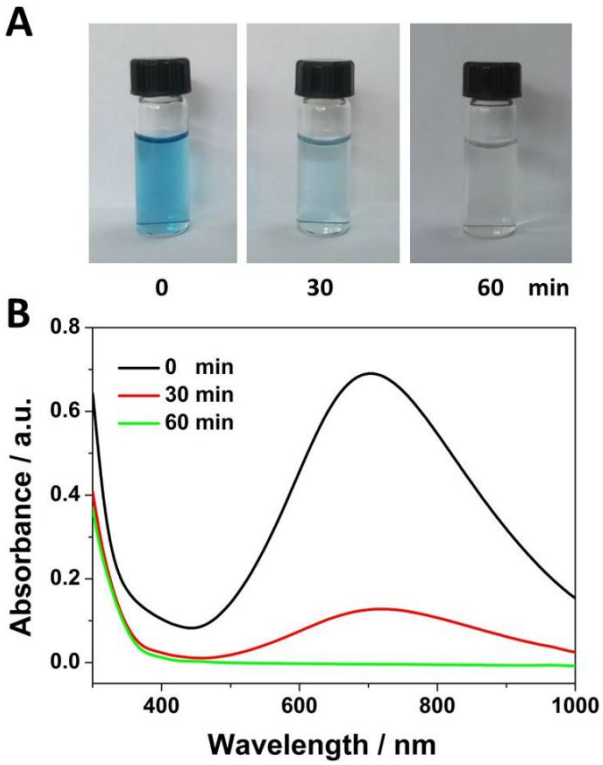

Figure S7. Confirmation of material conversion in the presence of Ag^+. (A) Photographs of aqueous dispersions of PB NPs (0.05 mg/mL) after incubation in Ag^+ solusions (5.0 μM) for

different times; (B) UV-vis adsorption spectra of the PB NPs dispersions after the incubation in Ag^+ solutions.

Confirmation of Sensing Principle of Silver Ions. The material conversion from photothermal PB to non-photothermal silver ferrocyanide in the presence of Ag^+ was confirmed by UV-vis adsorption spectroscopy as shown in Figure S7. PB NPs were incubated in Ag^+ solutions (5.0 μM) for different times to monitor their colorimetric and spectrophotometric changes. As can be seen, the color of the PB NPs dispersions degraded gradually with the increase of incubation time, which became colorless after the incubation for 1.0 hour. Meanwhile, the absorbance at 710 nm as well as in the NIR region (700-1000 nm) in UV-vis adsorption spectra of the PB NPs dispersions decreased dramatically with the increase of incubation time. These results confirmed the conversion of photothermal PB to colorless non-photothermal silver ferrocyanide in the presence of Ag^+. With a higher solubility product equilibrium constant (K_{sp}) and worse stability, PB ($Fe_4[Fe(CN)_6]_3$) was transformed to silver ferrocyanide ($Ag_4[Fe(CN)_6]_3$) in the presence of Ag^+ according to the dissolution-precipitation equilibrium mechanism.[7]

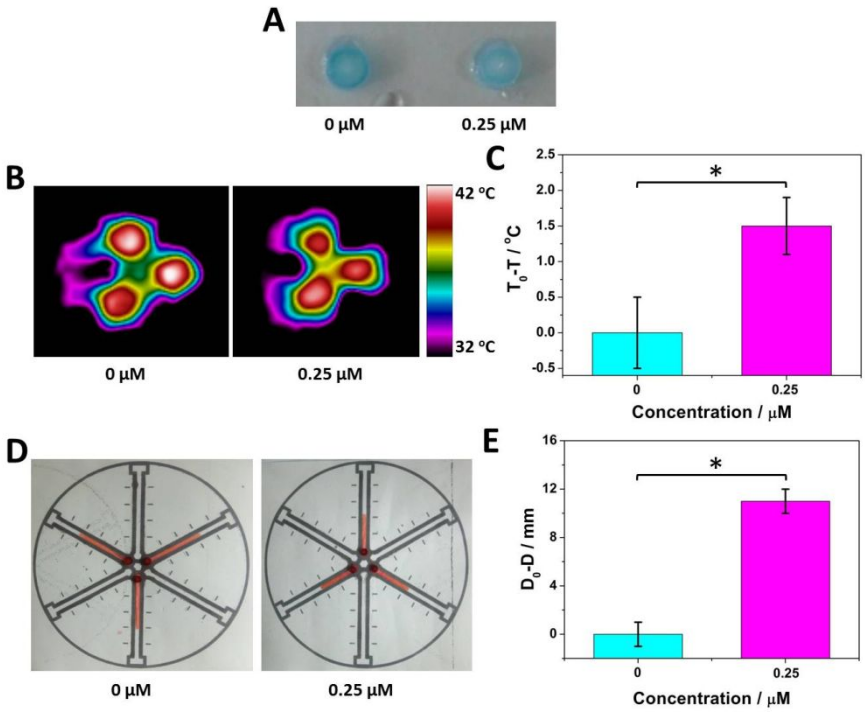

Figure S8. Determination of Ag^+ upon prolonging of sample-pretreatment time. (A) Photograph of the composite hydrogels after incubation in different concentrations of Ag^+ solutions for 10 hours; (B) Thermal images of the composite hydrogels after the laser irradiation for 60 s at a power density of 0.38 $W \cdot cm^{-2}$; (C) Relative temperature changes (T_0-T) of the hydrogels after the irradiation; (D) Photographs of the hydrogel-loaded μPADs after the irradiation; (E) Relative changes in on-chip travelling distance (D_0-D) of dye solutions after the irradiation. Error bars represent standard deviations (n=3). An asterisk indicates a statistically significant difference (*t-test*, $*P < 0.05$).

Determination of Ag^+ upon Prolonging of Sample-Pretreatment Time. To study the effect of sample-pretreatment time on detection limit of the photothermal μPAD for Ag^+ detection, the composite hydrogels were incubated in Ag^+ solutions (0.25 μM) for 10 hours. After the incubation, the composite hydrogels (0.25 μM) exhibited obviously degraded color in comparison with the control hydrogels (0 μM), as shown in Figure S8. After laser irradiaiton of the hydrogels on the μPAD, significant

difference between the control (0 μM) and the Ag^+-treated hydrogels (0.25 μM) was observed from both the thermal image- and distance-based readout results. Hence, Ag^+ can be quantitatively determined with lower detection limits by properly prolonging the incubation time of the composite hydrogels in Ag^+ solutions. It was worth noting that the control hydrogel displayed both lower temperature elevation and shorter on-chip dye-travelling distance in comparison with that of the control hydrogel with a shorter incubation time (i.e., 1.5 hours), which can be ascribed to the inevitable minor decomposition of PB at neutral conditions.

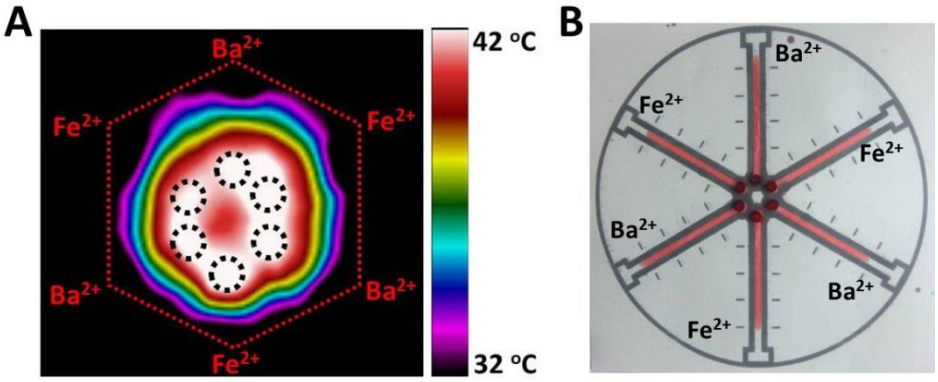

Figure S9. Selectivity of the photothermal μPAD towards Ba^{2+} and Fe^{2+}. (A) Thermal image of the Ba^{2+}- and Fe^{2+}-treated composite hydrogels after the laser irradiation for 60 s at a power density of 0.38 $W \cdot cm^{-2}$; (B) Photograph of the hydrogel-loaded μPAD after the irradiation.

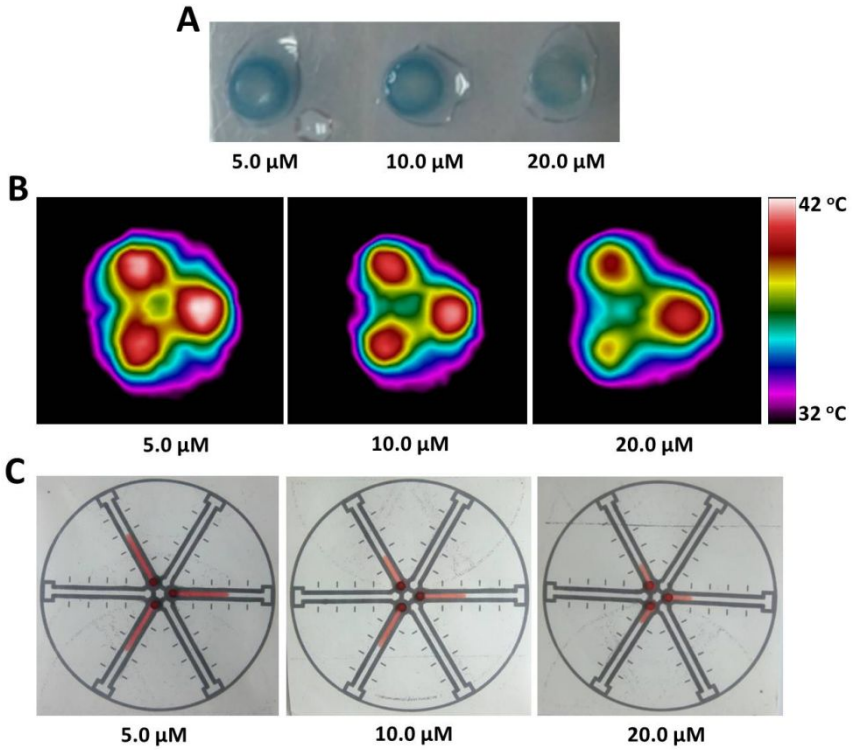

Figure S10. Determination of Ag^+ in real water samples. (A) Photograph of the composite hydrogels after incubation with water samples spiked with different concentrations of Ag^+ solutions; (B) Thermal images of the composite hydrogels after the laser irradiation for 60 s at a power density of 0.38 $W \cdot cm^{-2}$; (C) Photographs of the hydrogel-loaded μPADs after the irradiation.

Determination of Ag^+ in Real Water Samples. Real water samples were collected from a local lake (Jiulong Lake) and were diluted 5-fold with B-R buffer solutions (pH=7.2). The samples were then spiked with different concentrations of standard Ag^+ solutions to prepare water samples with final Ag^+ concentrations of 5.0, 10, 20 μM, respectively. After incubation of the composite hydrogels in the water samples, Ag^+ concentrations were determined on the photothermal μPAD using the dual-mode readout method. As shown in Figure S10, with the increase of Ag^+ concentration in the water samples, the

composite hydrogels exhibited increasingly degraded color. In addition, the quantitative detection results acquired from both the thermal image- and distance-based readout methods were in good agreement with the results obtained from Figure 5.

Table S1. Determination of Ag^+ in spiked real water samples using the thermal image-based readout method on the photothermal μPAD (n=4).

Sample number	Spiked concentration (μM)	Detected concentration (μM)	Recovery (%)	RSD (%)
1	5.0	4.79±0.10	95.8	2.09
2	10	10.2±0.55	101.8	5.40
3	20	19.5±0.90	97.5	4.62

Table S2. Determination of Ag^+ in spiked real water samples using the distance-based readout method on the photothermal μPAD (n=4).

Sample number	Spiked concentration (μM)	Detected concentration (μM)	Recovery (%)	RSD (%)
1	5.0	4.79±0.20	95.8	3.97
2	10	9.55±0.65	95.5	6.81
3	20	19.3±1.6	96.3	8.10

References

(1) Niedl, R. R.; Beta, C. Hydrogel-driven paper-based microfluidics. *Lab Chip* **2015**, 15, 2452-2459.

(2) Fu, G.; Liu, W.; Feng, S.; Yue, X. Prussian blue nanoparticles operate as a new generation of photothermal ablation agents for cancer therapy. *Chem. Commun.* **2012**, 48, 11567-11569.

(3) Fu, G.; Liu, W.; Li, Y.; Jin, Y.; Jiang, L.; Liang, X.; Feng, S.; Dai, Z. Magnetic Prussian blue nanoparticles for targeted photothermal therapy under magnetic resonance imaging guidance. *Bioconjugate Chem.* **2014**, 25, 1655-1663.

(4) Fu, G.; Sanjay, S. T.; Dou, M.; Li, X. Nanoparticle-mediated photothermal effect enables a new method for quantitative biochemical analysis using a thermometer. *Nanoscale* **2016**, 8, 5422-5427.

(5) Zhu, C.; Lu, Y.; Chen, J.; Yu, S. Photothermal Poly(N-isopropylacrylamide)/Fe3O4 Nanocomposite Hydrogel as a Movable Position Heating Source under Remote Control. *Small* **2014**, 10, 2796-2800.

(6) Zhu, C.; Lu, Y.; Peng, J.; Chen, J.; Yu, S. Photothermally Sensitive Poly(N-isopropylacrylamide)/Graphene Oxide Nanocomposite Hydrogels as Remote Light-Controlled Liquid Microvalves. *Adv. Funct. Mater.* **2012**, 22, 4017-4022.

(7) Huang, W.; Liang, Y.; Deng, Y.; Cai, Y.; He, Y. Prussian Blue nanoparticles as optical probes for visual and spectrophotometric determination of silver ions. *Microchim. Acta* **2017**, 184, 2959-2964.